

Magnetic Energy Conversion in MHD: Curvature Relaxation and Perpendicular Expansion of Magnetic Fields

SENBEI DU,¹ HUI LI,¹ XIANGRONG FU,² ZHAOMING GAN,² AND SHENGTAI LI¹

¹*Los Alamos National Laboratory, Los Alamos, NM 87545, USA*

²*New Mexico Consortium, Los Alamos, NM 87544, USA*

ABSTRACT

The mechanisms and pathways of magnetic energy conversion are an important subject for many laboratory, space and astrophysical systems. Here, we present a perspective on magnetic energy conversion in MHD through magnetic field curvature relaxation (CR) and perpendicular expansion (PE) due to magnetic pressure gradients, and quantify their relative importance in two representative cases, namely 3D magnetic reconnection and 3D kink-driven instability in an astrophysical jet. We find that the CR and PE processes have different temporal and spatial evolution in these systems. The relative importance of the two processes tends to reverse as the system enters the nonlinear stage from the instability growth stage. Overall, the two processes make comparable contributions to the magnetic energy conversion with the PE process somewhat stronger than the CR process. We further explore how these energy conversion terms can be related to particle energization in these systems.

(This is the Accepted Manuscript version of an article accepted for publication in *The Astrophysical Journal*. IOP Publishing Ltd is not responsible for any errors or omissions in this version of the manuscript or any version derived from it.)

1. INTRODUCTION

The energization and heating of plasma is a universal phenomenon in laboratory, space physics and astrophysics, such as in the solar corona, solar wind, disks around active galactic nuclei, astrophysical jets, etc. Magnetic energy is frequently found to be the free energy source for energizing plasma in these systems and thus the conversion of magnetic energy is a key element for understanding these plasma systems (e.g., [Parker 1979](#); [Colgate et al. 2001](#); [Kronberg et al. 2001](#)). Observations of many magnetically dominated astrophysical environments and systems have demonstrated fast magnetic energy release and strong particle acceleration. Blazar jets powered by supermassive black holes can exhibit \sim minutes variations in TeV emissions ([Aharonian et al. 2007](#)) and gamma-ray flares from Crab nebula have been observed as well ([Abdo et al. 2011](#)).

For example, one commonly considered case is magnetic reconnection as one of the most important magnetic energy conversion processes. The rapid change in magnetic field connectivity converts magnetic energy stored in anti-parallel magnetic field into plasma energy (e.g., [Sweet 1958](#); [Parker 1957, 1963](#); [Priest & Forbes 2007](#); [Birn et al. 2012](#)) and can lead to efficient particle acceleration and heating (e.g., [Drake et al. 2006](#); [Li et al. 2019](#)). In addition, it is well established that magnetic reconnection occurring in global-scale current sheets can contribute to the energy release in solar flares and the Earth magnetosphere ([Dungey 1961](#)). More recently, [Ripperda et al. \(2020\)](#) demonstrate with general-relativistic resistive MHD simulations that magnetic reconnection can generate plasmoids and explain black hole flares. Another important case is the kink-instability enabled magnetic energy conversion. In astrophysical jets, the free magnetic energy can also be stored in large-scale helical magnetic fields and is released due to kink instability (e.g., [Li et al. 2006](#); [Nakamura et al. 2007](#); [Mizuno et al. 2009](#); [Zhang et al. 2017](#)). The third case that is often studied is the magnetized turbulence in which the injected magnetic energy can be converted to plasma energy as well. Here, the compression effect has been discussed in the context of single-fluid MHD and it is especially important for the plasma heating ([Birn et al. 2012](#); [Du et al. 2018](#)). In particular, it was proposed (e.g., [Yang et al. 2016](#); [Matthaeus et al. 2020](#)) that the electromagnetic energy interconverts with the flow kinetic energy via the $\mathbf{j} \cdot \mathbf{E}$ term and the “pressure-strain” interaction converts energy between flow kinetic energy and the internal energy. The pressure-strain interaction consists both

a compressive part $-p\nabla \cdot \mathbf{u}$ [pressure dilatation, [Aluie et al. \(2012\)](#)] and a “Pi-D” term which is the product of a traceless pressure tensor and the velocity shear tensor, though its robustness may continue to be under scrutiny ([Du et al. 2020](#)).

Rapid progress has also been made in the area of plasma kinetic studies of magnetic reconnection and the associated particle energization along with theoretical developments (e.g., [Sironi & Spitkovsky 2014](#); [Guo et al. 2014](#); [Dahlin et al. 2014](#); [Zank et al. 2014](#); [Werner et al. 2016](#); [Li et al. 2015, 2017, 2018, 2019](#); [le Roux et al. 2015, 2018](#); [Lazarian et al. 2020](#)). In particular, [Li et al. \(2017\)](#) constructed the electric current from various particle drift motions and evaluate the particle energization due to drifts in kinetic particle-in-cell (PIC) simulations of magnetic reconnection. While curvature drift is found to be the dominant particle acceleration mechanism, other drifts also have some minor contributions. Of particular importance is the gradient (or grad-B) drift, which usually has an decelerating effect and counteracts with the curvature drift acceleration. [Li et al. \(2018\)](#) further show that combining the various drift acceleration terms yields an expression for the energization that can be interpreted as the summation of fluid compression, shear, and inertial energization effects. In addition to the first-principle kinetic studies, the usage of the test particle approach in reconnection and kink configurations (e.g., [Kowal et al. 2012](#); [Medina-Torrejón et al. 2021](#)) has also yielded useful understanding in particle energization processes.

Connecting the microscopic particle motion and acceleration processes with the macroscopic magnetic energy conversion processes remains a long-standing challenge. [Beresnyak & Li \(2016\)](#) discussed the conversion of magnetic energy in MHD and its relation to the first-order Fermi particle acceleration. Their analysis suggests that the energy transfer from magnetic field to kinetic motions is inherently related to the curvature drift acceleration. [Beresnyak & Li \(2016\)](#) also discuss the distinction between different types of turbulence. Specifically, the energization in decaying magnetic turbulence and magnetic reconnection driven turbulence are compared against each other using incompressible MHD simulations. While both systems see a conversion of magnetic energy into kinetic energy, the magnetic reconnection case is found to have a stronger energization. This is likely due to the larger free magnetic energy that is available in the reconnection case. In terms of the curva-

ture drift, one may argue that the magnetic field possesses “good” curvature that helps the release of magnetic energy and particle acceleration during reconnection. However, as we will show in this paper, the conclusions made by [Beresnyak & Li \(2016\)](#) are contingent on the incompressible nature of the flow and need to be revisited for a general compressible plasma.

In this paper, we will present detailed analyses of the magnetic energy conversion processes in two typical configurations, reconnection and kink, using 3D MHD simulations. We show that two dominant processes can be identified in regulating the magnetic energy conversion. We will present results from the theoretical analysis in §2 and the numerical analysis in §3. Summary and conclusions are given in §4.

2. ENERGY CONVERSION IN MHD

2.1. *Two processes in magnetic energy conversion*

The ideal MHD energy equations, including magnetic energy and plasma energy, are

$$\frac{\partial}{\partial t} \left(\frac{B^2}{8\pi} \right) + \nabla \cdot \left[\frac{-(\mathbf{u} \times \mathbf{B}) \times \mathbf{B}}{4\pi} \right] = -\mathbf{j} \cdot \mathbf{E}; \quad (1)$$

$$\frac{\partial}{\partial t} \left(\frac{1}{2} \rho u^2 + \frac{p}{\gamma - 1} \right) + \nabla \cdot \left[\left(\frac{1}{2} \rho u^2 + \frac{\gamma p}{\gamma - 1} \right) \mathbf{u} \right] = \mathbf{j} \cdot \mathbf{E}. \quad (2)$$

We use the CGS Gaussian unit system throughout the paper. As usual, the quantities in the equations are defined as magnetic field \mathbf{B} , electric field \mathbf{E} , current density \mathbf{j} , plasma mass density ρ , flow velocity \mathbf{u} , thermal pressure p , and adiabatic index γ . The work done by the electric field $\mathbf{j} \cdot \mathbf{E}$ converts the magnetic energy to the plasma energy, and thus contributes to the energization of plasma. It can be expanded as

$$\mathbf{j} \cdot \mathbf{E} = -(\mathbf{u} \times \mathbf{B}) \cdot \frac{\nabla \times \mathbf{B}}{4\pi} = \frac{1}{4\pi} \mathbf{u} \cdot (\mathbf{B} \cdot \nabla \mathbf{B}) - \mathbf{u} \cdot \nabla \left(\frac{B^2}{8\pi} \right). \quad (3)$$

We further expand the first term on the right hand side of Equation (3) as

$$\frac{1}{4\pi} \mathbf{u} \cdot (\mathbf{B} \cdot \nabla \mathbf{B}) = \frac{1}{4\pi} (\mathbf{u} \cdot \mathbf{B})(\mathbf{b} \cdot \nabla B) + \frac{B^2}{4\pi} \mathbf{u} \cdot \boldsymbol{\kappa}, \quad (4)$$

where the magnetic field curvature is defined as $\boldsymbol{\kappa} = \mathbf{b} \cdot \nabla \mathbf{b}$ and $\mathbf{b} = \mathbf{B}/B$ is the unit vector tangent to the magnetic field. Combining these terms, we can re-cast Equation (3) as

$$\mathbf{j} \cdot \mathbf{E} = \frac{B^2}{4\pi} \mathbf{u} \cdot \boldsymbol{\kappa} - \mathbf{u} \cdot \nabla_{\perp} \left(\frac{B^2}{8\pi} \right). \quad (5)$$

Here, we denote the gradients parallel and perpendicular to the magnetic field as $\nabla_{\parallel} = \mathbf{b}(\mathbf{b} \cdot \nabla)$ and $\nabla_{\perp} = \nabla - \nabla_{\parallel}$. The equation shows that the total magnetic energy transfer in Equation (1) can be decomposed into two parts. Physically, the first term corresponds to the relaxation of high magnetic field line tension – curvature relaxation (CR) when the flow velocity is along the curvature of magnetic field, which releases magnetic energy. The second term corresponds to the perpendicular expansion (PE) of the magnetic energy, which can drive flows in the opposite direction of the magnetic energy gradient, releasing magnetic energy.

A complementary view is expressed via plasma energization by several previous studies (e.g., [Birn et al. 2012](#); [Du et al. 2018](#)) where Equation (2) can be rewritten as the plasma flow energy and thermal energy evolution,

$$\frac{\partial}{\partial t} \left(\frac{1}{2} \rho u^2 \right) + \nabla \cdot \left(\frac{1}{2} \rho u^2 \mathbf{u} \right) = \mathbf{j} \cdot \mathbf{E} - \mathbf{u} \cdot \nabla p; \quad (6)$$

$$\frac{\partial}{\partial t} \left(\frac{p}{\gamma - 1} \right) + \nabla \cdot \left(\frac{\gamma p}{\gamma - 1} \mathbf{u} \right) = \mathbf{u} \cdot \nabla p. \quad (7)$$

These equations suggest that the work done by the electric field $\mathbf{j} \cdot \mathbf{E}$ contributes strictly to the bulk acceleration in ideal MHD and heating is only facilitated by compression $\mathbf{u} \cdot \nabla p$.

2.2. The role of fluid compression and shear

Another way to express $\mathbf{j} \cdot \mathbf{E}$ is by using the perpendicular velocity \mathbf{u}_{\perp} in the place of the total velocity \mathbf{u} since the parallel velocity does not contribute to the electric field. It can be shown that the curvature drift term is related to the flow shear as

$$\frac{B^2}{4\pi} \mathbf{u} \cdot \boldsymbol{\kappa} = -\frac{B^2}{4\pi} \mathbf{b}\mathbf{b} : \nabla \mathbf{u}_{\perp},$$

and that the total $\mathbf{j} \cdot \mathbf{E}$ is decomposed into the sum of perpendicular expansion and shear,

$$\mathbf{j} \cdot \mathbf{E} = -\mathbf{u}_{\perp} \cdot \nabla \left(\frac{B^2}{8\pi} \right) - \frac{B^2}{4\pi} \mathbf{b}\mathbf{b} : \nabla \mathbf{u}_{\perp}, \quad (8)$$

or

$$-\mathbf{j} \cdot \mathbf{E} = \nabla \cdot \left(\frac{B^2}{8\pi} \mathbf{u}_\perp \right) - \frac{B^2}{8\pi} \frac{\nabla \cdot \mathbf{u}_\perp}{3} + \frac{B^2}{4\pi} \mathbf{b}\mathbf{b} : \boldsymbol{\sigma}, \quad (9)$$

where $\sigma_{ij} = (1/2)(\partial_i u_{\perp j} + \partial_j u_{\perp i} - 2\nabla \cdot \mathbf{u}_\perp \delta_{ij}/3)$ is the shear tensor (δ_{ij} is the Kroneker delta). Equation (9) is very reminiscent of the results obtained by Li et al. (2018), who show from the Vlasov equation that in the limit of a gyrotropic (aka CGL) pressure (Chew et al. 1956; Hunana et al. 2019), the plasma energization in the perpendicular direction $\mathbf{j}_\perp \cdot \mathbf{E}_\perp$ can be expressed as the sum of a compression term, a shear term, and an inertial term [see their Equation (9) in Li et al. (2018) where \mathbf{j}_\perp is the perpendicular component of the current density w.r.t to the local magnetic field and such a current is produced by various particle motions and drifts]. Similarly in our Equation (9), the first term on the right does not contribute to magnetic energy conversion, the second and third terms correspond to magnetic energy conversion via flow expansion/compression and flow shear, respectively.

The fact that Equations (5) and (9) are mathematically equivalent suggests that both CR and PE processes are mixed together in the shear term in Equation (9). In this paper, we opt to use Equation (5) as our primary approach to analyze the magnetic conversion processes.

3. MHD SIMULATIONS

In this section, we demonstrate how magnetic energy conversion occurs in different types of systems, namely magnetic reconnection and kink-unstable jet. We have performed a set of 3D ideal MHD simulations using the *Athena++* code (Stone et al. 2008, 2020) and the *LA-COMPASS* code to study these systems. We focus on the temporal and spatial evolution of the main terms described in Equation (5).

3.1. Magnetic reconnection

The magnetic reconnection simulation is initialized with force-free current sheets with the following magnetic field configuration,

$$B_x = B_0 \tanh \left[\frac{d}{\pi L} \sin \left(\frac{\pi z}{d} \right) \right]; \quad B_y = B_0 \sqrt{1 + \left(\frac{B_g}{B_0} \right)^2 - \tanh^2 \left[\frac{d}{\pi L} \sin \left(\frac{\pi z}{d} \right) \right]}; \quad B_z = 0. \quad (10)$$

Here, B_0 is the strength of the upstream reconnecting magnetic field; B_g is the guide field strength; L is the half thickness of the current sheets; and d is the distance between two adjacent current sheets. We use a box size of 2π in all three directions for our simulation, resolved by 512^3 cells. The boundary conditions are periodic in all directions. We choose the parameters $B_0 = 1$, $B_g = 0$, $L = 0.05$, and $d = \pi$ so that there are two current sheets initially. The initial density and temperature profiles are both uniform. The simulation is normalized such that the initial Alfvén speed $V_A = 1$ and the initial plasma $\beta = 0.2$ (ratio between the thermal pressure and magnetic pressure). An adiabatic equation of state is used with an adiabatic index $= 5/3$. The characteristic Alfvén time will be $\tau_A = 2\pi$. The current sheets are perturbed initially by random Alfvénic fluctuations that propagate in the xy -plane. We introduce 100 random sine waves with transverse velocity and magnetic fluctuations δV_z and δB_z that are correlated in an Alfvénic fashion ($\delta V_z = \pm \delta B_z$). The total perturbation rms amplitude is $\sim 8\%$ and the cross helicity is close to zero. The perturbation is restricted to long-wavelength fluctuations with the wavelength equal or longer than a third of the box size.

We note that although we use ideal MHD without explicit resistivity and viscosity in the simulation, magnetic reconnection can still occur due to numerical diffusivity at the grid scale. In a high-Lundquist number plasma typical for space and astrophysical environments, the energy conversion is dominated by ideal MHD process and resistive heating can generally be neglected at large scales. For magnetic reconnection, the nonideal physics is important in the diffusion region where the magnetic field lines break, but the energy conversion process for the entire current sheet system is not sensitive to the nonideal physics. We do caution that due to the limited spatial resolution, our simulation corresponds to a moderate Lundquist number on the order of hundreds. It is unclear at this point how our results hold in higher Lundquist number regimes where the plasmoid instability becomes dominant (Loureiro et al. 2007; Bhattacharjee et al. 2009; Huang & Bhattacharjee 2010; Yang et al. 2020).

Figure 1 plots the energy conversion terms as in Equation (5) in the top panel. The evolution of energy in the z -component of the magnetic field normalized to the initial magnetic energy is shown in the bottom panel, which also includes the evolution of total magnetic energy, kinetic energy, and

internal energy. Based on our simulation, we find that the evolution may be separated into two stages. During the first stage, the evolution is characterized by a linear instability, which occurs at time $t \lesssim 4$ as indicated by the initial exponential growth of energy in B_z magnetic field. For the second stage at later time, the growth rate slows down though the magnetic energy is still being released. As illustrated by the top panel of Figure 1, the CR term appears to be dominant in energy conversion at the beginning of the first stage ($t \lesssim 2$). At later time, however, the PE term becomes more important. The overall conversion of magnetic field is mostly contributed by the PE term at the end of the simulation.

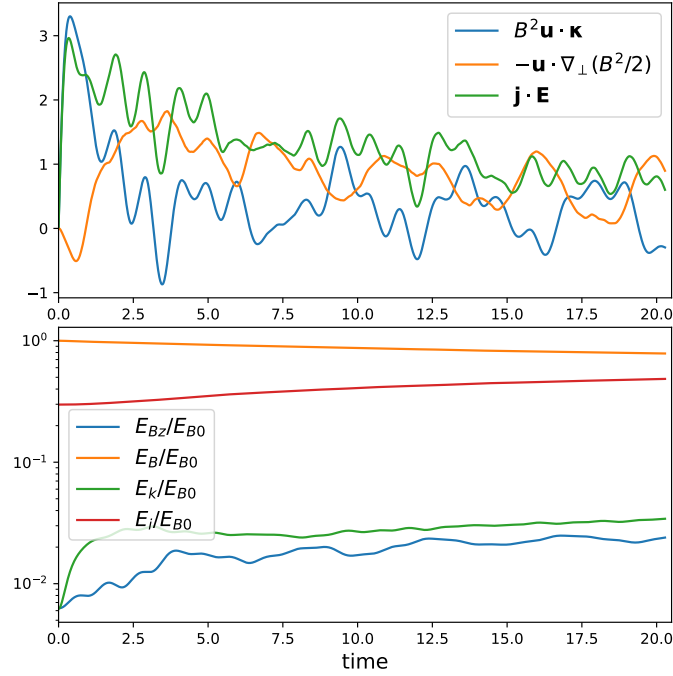


Figure 1. Top panel: time history of energization terms in Equation (5) for the magnetic reconnection simulation, including the curvature related term $(B^2/4\pi)\mathbf{u} \cdot \boldsymbol{\kappa}$, the gradient related term $-\mathbf{u} \cdot \nabla_{\perp}(B^2/8\pi)$, and the total energization $\mathbf{j} \cdot \mathbf{E}$. All these terms are integrated over the entire simulation box. Bottom panel: evolution of different energy components as reconnection proceeds, including the z -component of magnetic field, total magnetic field, total kinetic energy, and internal energy. All the energies are normalized to the initial magnetic energy.

Next, we look into the spatial distribution of the energy conversion terms. Figure 2 displays the spatial distribution of the CR and PE terms and their sum in the x - z plane. Examples from the

early ($t = 1.0$) and late ($t = 16.0$) stages are shown in the figure. We find that during the first stage, the strong magnetic energy conversion due to relaxation of magnetic field curvature occurs near the reconnection X-line and the ends of magnetic islands formed in the two main current sheets. It is interesting to note that there is an approximate spatial anti-correlation between the CR and PE terms, although the CR term is stronger overall. During the second stage, both conversion terms appear to be turbulent, as there are small positive or negative patches mixed in the reconnection and (3D) flux rope regions. The amplitude of the PE term becomes much stronger and the global summation also indicates its dominance.

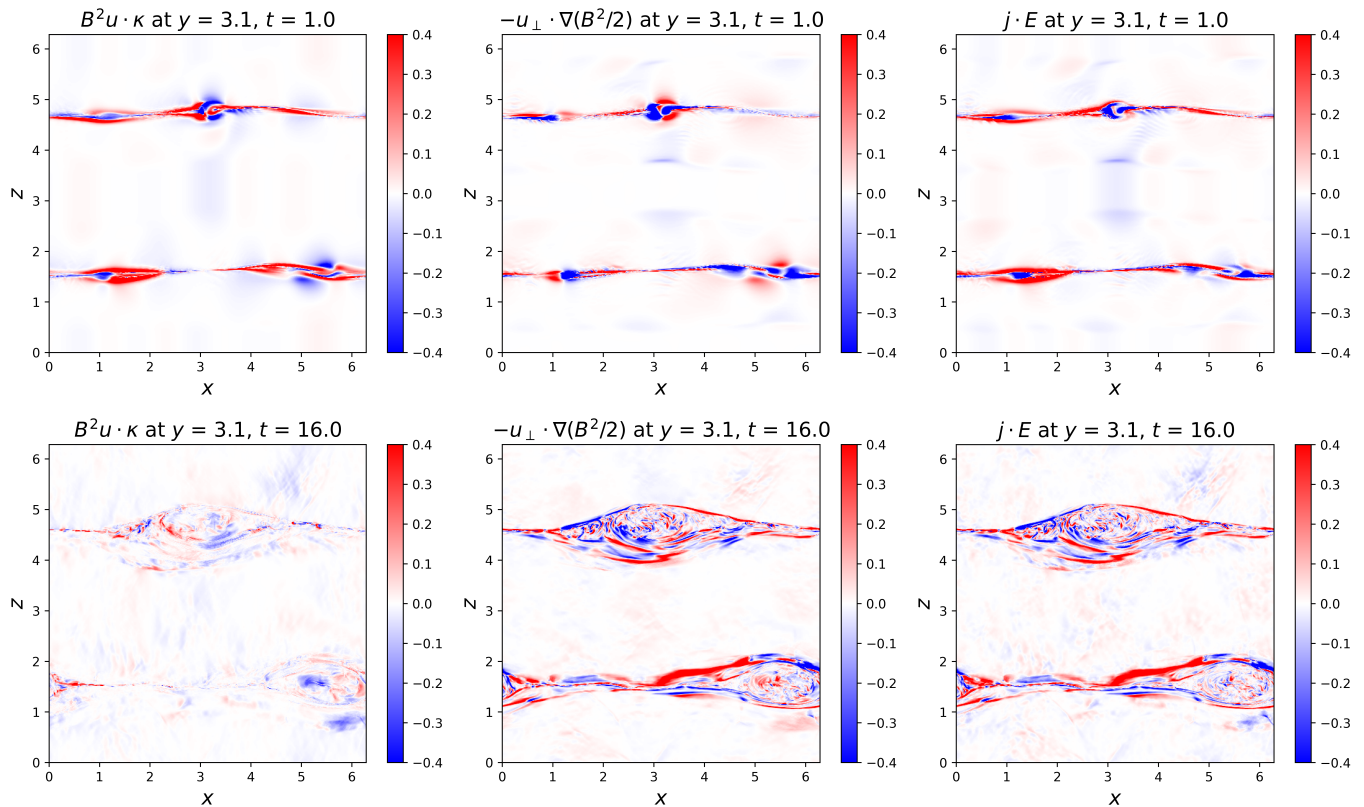


Figure 2. Spatial distribution of the CR (left) and PE (middle) terms in the x - z plane at early ($t = 1.0$) and late ($t = 16.0$) times of the magnetic reconnection simulation. The right panels show the total energization as the sum of the CR and PE terms.

To further illustrate the time evolution of the energy conversion terms, the probability density functions (pdfs) of the curvature magnitude κ and the cosine of the angle between the velocity and

curvature vector $\cos \theta_{u\kappa}$ are shown in Figure 3. The pdfs are calculated by the computational cell-based quantities. The velocity distribution does not change much throughout the simulation and is not shown here. The curvature distribution extends to large curvature values and develops power law like distributions in the low and high curvature ranges, similar to those reported by Yang et al. (2019); Bandyopadhyay et al. (2020) in turbulence simulations and observations. The pdfs of $\cos \theta_{u\kappa}$ show that at the early stage, the angle $\theta_{u\kappa}$ concentrates near 0° and 180° due to the reconnection inflow and outflow. The correlation between velocity and curvature directions degrades over time as the distribution becomes more random and tends toward zero. This is probably the reason why the magnetic energy conversion due to curvature relaxation becomes less dominant later in the simulation.

Similarly, we can also inspect the pdfs of the perpendicular gradient $\nabla_\perp(B^2/2)$ and the angle it makes with the velocity $\theta_{u\nabla_\perp}$, as shown in Figure 4. The correlation between the velocity and perpendicular gradient vectors also degrades over time. Unlike the curvature distribution, however, the pdf of $|\nabla_\perp(B^2/2)|$ develops a “bump” starting at high values ~ 0.5 , which leads to the dominance of the perpendicular expansion process. This bump comes from the turbulent patches as shown in the lower right panel of Figure 2.

Figure 5 shows the pdfs of the two conversion terms in Equation (5) at two different time frames. At an earlier time ($t = 1$), the distributions of both terms are clearly skewed, suggesting systematic effects of the positive velocity-curvature correlation and perpendicular fluid compression. In contrast, at a later time ($t = 16$), both pdfs appear to be more symmetric about zero due to the more turbulent nature of the system. The insets show the cumulative partial moments $PM(x) = \int_{-\infty}^x x' f(x') dx'$ with $f(x')$ being the pdf of $B^2 \mathbf{u} \cdot \boldsymbol{\kappa}$ or $-\mathbf{u} \cdot \nabla_\perp(B^2/2)$. Although most of the cells have nearly zero contribution to the energization as indicated by the sharp peaks in the pdfs, the partial moments illustrate that the cells with $-\mathbf{u} \cdot \nabla_\perp(B^2/2) \geq 0.5$ contribute significantly to the total magnetic energy conversion. These analyses strongly suggest that the overall magnetic energy conversion in 3D reconnection is actually dominated by the development of turbulent patches inside the flux ropes undergoing perpendicular expansion owing to the magnetic pressure gradients. These patches

could be consequences of collisions between reconnection outflows as well as secondary instabilities as discussed in Huang & Bhattacharjee (2016); Kowal et al. (2017); Yang et al. (2020).

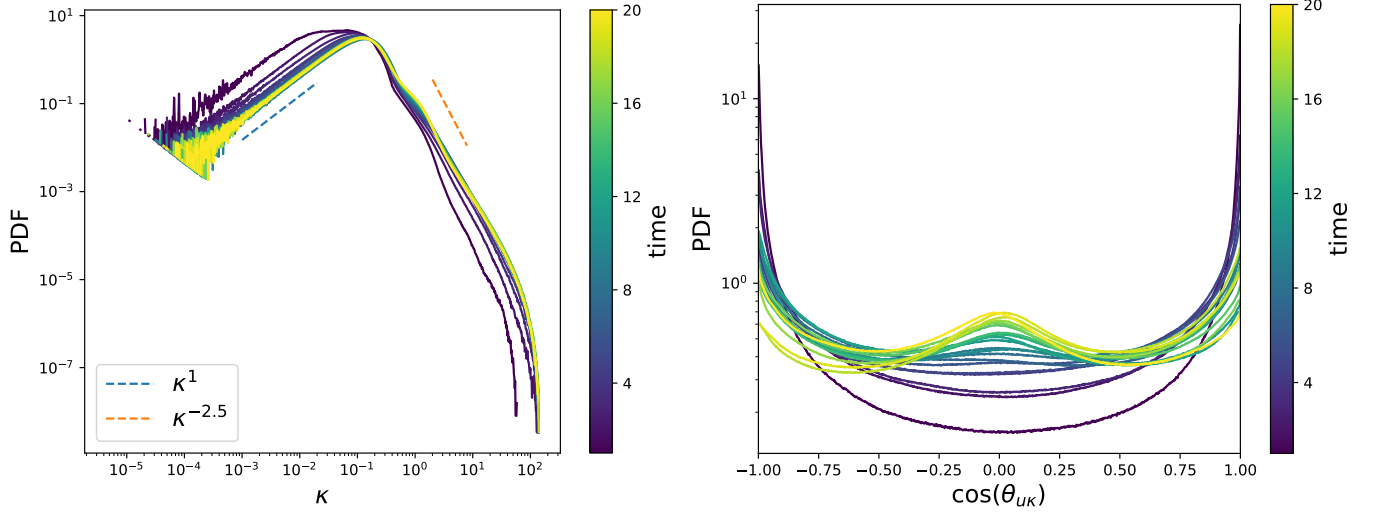


Figure 3. The probability density functions of κ and $\cos \theta_{u\kappa}$ in the reconnection simulation. The colormap represent time evolution.

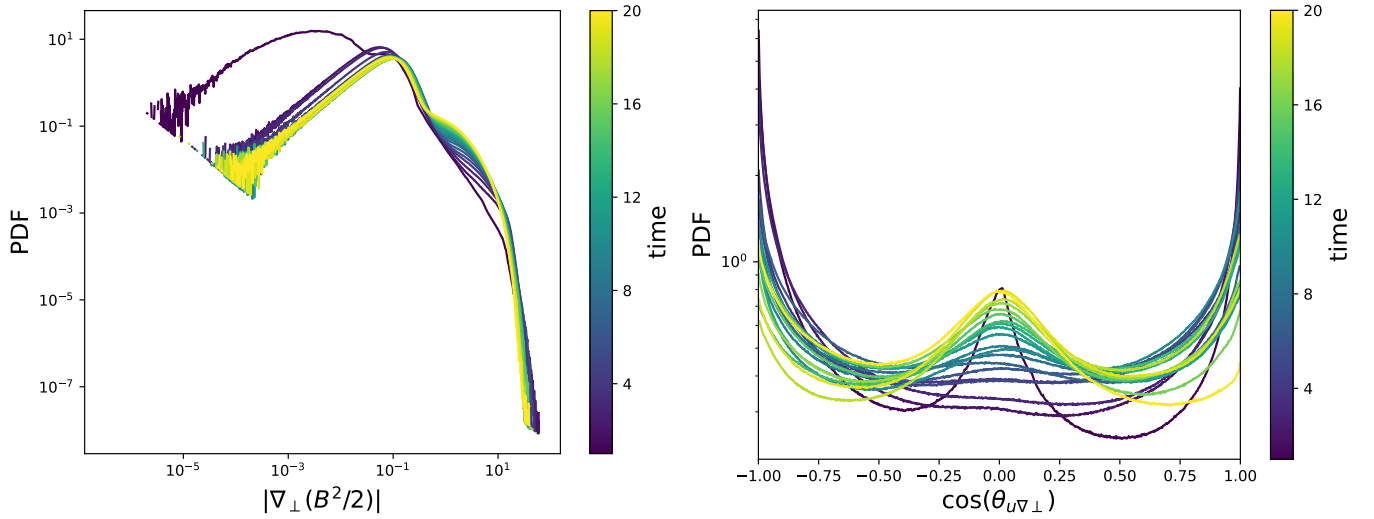


Figure 4. Similar to Figure 3, but for the pdfs of $|\nabla_{\perp}(B^2/2)|$ and $\cos \theta_{u\nabla_{\perp}}$ (where $\theta_{u\nabla_{\perp}}$ is the angle between \mathbf{u} and $\nabla_{\perp}(B^2/2)$) in the reconnection simulation. The colormap represent time evolution.

To further investigate how the CR and PE terms behave under different conditions, we have studied a 3D reconnection set-up with a guide field $B_g = 0.2$ using Equation ((10)). This is the same set-up as

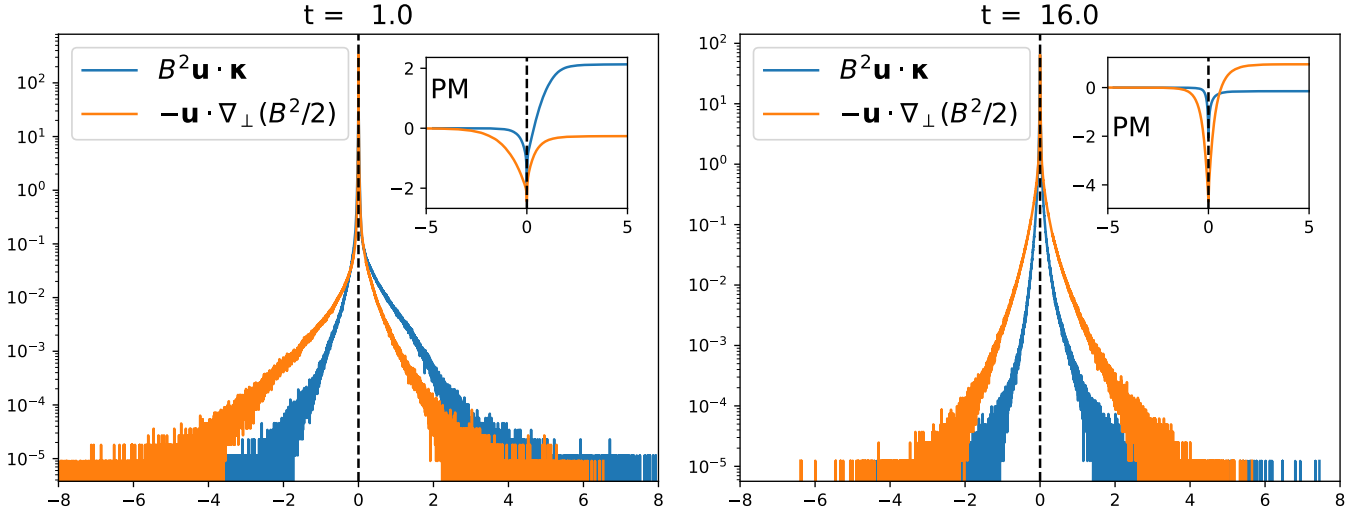


Figure 5. The probability density functions of the two energization terms $B^2 \mathbf{u} \cdot \boldsymbol{\kappa}$ and $-\mathbf{u} \cdot \nabla_{\perp} (B^2/2)$ in the reconnection simulation at early and late times. The insets show the cumulative partial moments (PM) from the two terms (see text for the definition).

given in a 3D particle-in-cell (PIC) simulation presented by [Li et al. \(2019\)](#). The PIC simulation has a similar initial magnetic field configuration as our MHD simulation, though with only one current sheet, and the box size is $150d_i \times 75d_i \times 62.5d_i$ where d_i is the ion inertial length. [Figure 6](#) shows the evolution of both CR and PE terms, though interestingly the curvature relaxation term appears to be slightly more important overall. This is different from the case when the guide field $B_g = 0$. We note that the normalization here is different from the MHD simulation. The velocity is normalized to the speed of light and length to the electron inertial length d_e . The electron plasma frequency ω_{pe} is set equal to the electron cyclotron frequency Ω_{ce} , which is defined by the magnetic field strength in the reconnection (x - z) plane. The ion-to-electron mass ratio is set to 25 so that the Alfvén speed is $V_A \simeq d_i \Omega_{ci} = 0.2c$. We have verified that including the same guide field in the 3D MHD reconnection simulation will also enhance the relative importance of the curvature relaxation term. The physical reason may be that a guide field component can suppress the expansion of magnetic field line perpendicular to the upstream magnetic field. [Figure 7](#) shows the history of the energization terms for two runs with $\beta = 0.5$. The format is the same as [Figure 1](#). The case without guide field is shown in the left panel and the case with a guide field $B_g = 0.2B_0$ is shown in the right panel. The

general evolution of these cases are similar to the $\beta = 0.2$ run. Figure 8 plots the fraction of the CR and PE contributions to the total energization (cumulative in time), which illustrates more clearly that the inclusion of a guide field enhances the relative importance of the curvature relaxation term.

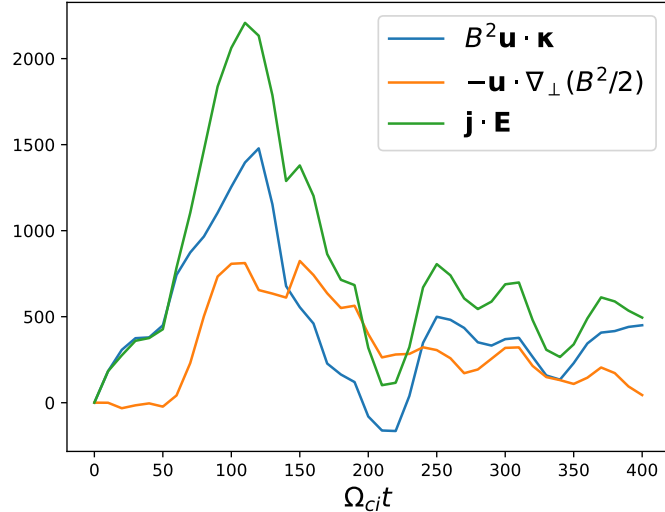


Figure 6. Decomposition of the $\mathbf{j} \cdot \mathbf{E}$ term using the 3D PIC simulation by Li et al. (2019) which has a guide field of $B_g = 0.2$. This guide field weakens the effect of the PE process, making the CR process more dominant.

3.2. Kink jet

Another common astrophysical system that may lead to strong magnetic energy conversion is kink instability in astrophysical jets. Here, we present a relativistic MHD simulation of a kink unstable jet following the setup in Mizuno et al. (2009) and Zhang et al. (2017). The magnetic field has the form of

$$B_z = \frac{B_0}{1 + (r/r_0)^2}; B_\phi = \frac{B_0}{1 + (r/r_0)^2} \left(\frac{r}{r_0} \right),$$

where we use $B_0 = 2$ and $r_0 = 1$; r is the radial distance to the central axis. The simulation box size is 40 in x and y directions with 640 cells each and 64 in z direction with 1024 cells. Periodic boundaries are used in z direction and outflow boundaries in x and y directions. The system is perturbed by random velocity fluctuations of $0.01 c$ ($c = 1$ in the simulation). The simulation is run until the time of 350. The initial density ρ and pressure p are uniform ($\rho = 1$ and $p = 0.01$), and

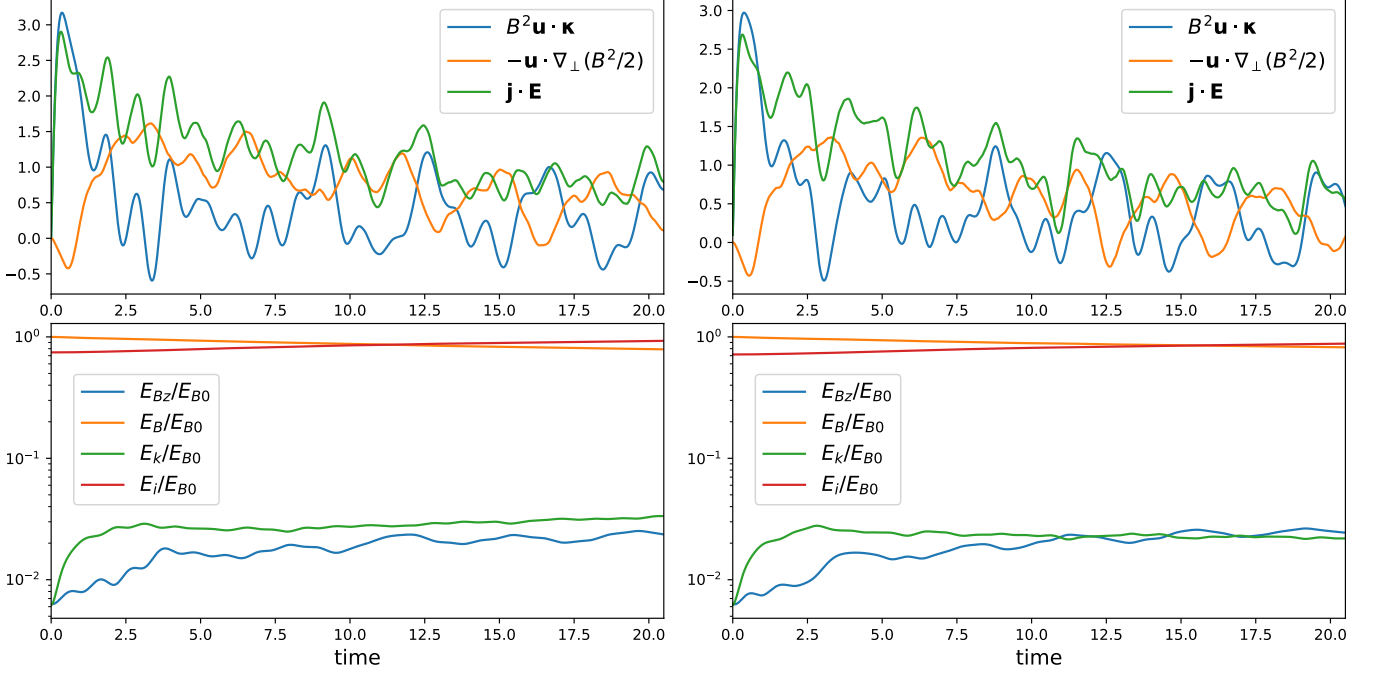


Figure 7. History of the energization terms similar to Figure 1, but for $\beta = 0.5$. The left panel is for the case without guide field and the right panel has a guide field of $B_g = 0.2B_0$.

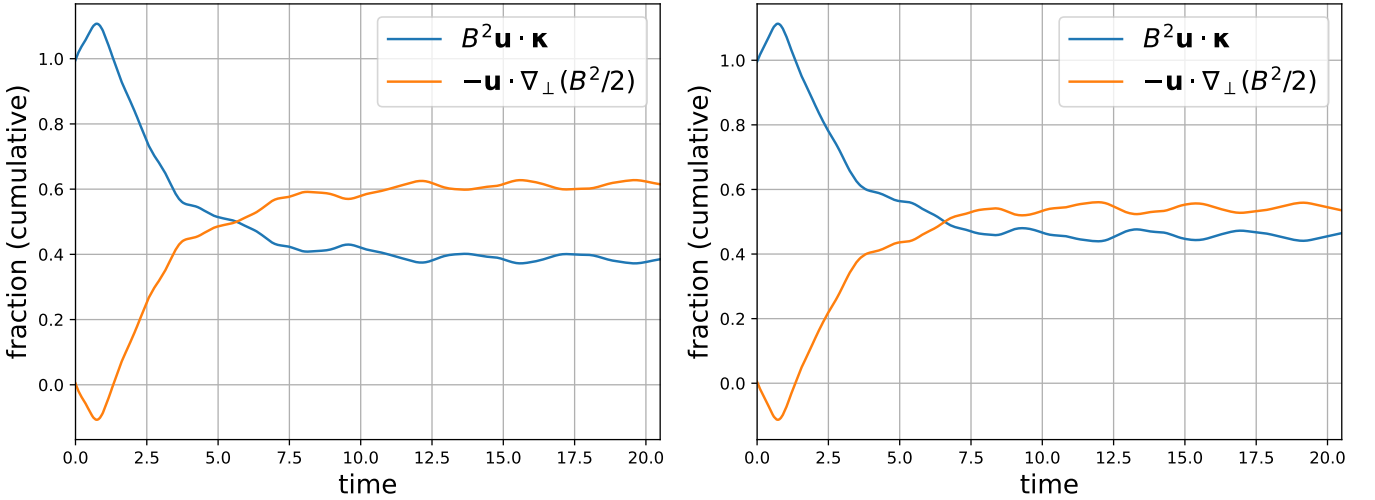


Figure 8. Fractions of the energization terms in total $\mathbf{j} \cdot \mathbf{E}$ for $\beta = 0.5$. The left panel is for the case without guide field and the right panel has a guide field of $B_g = 0.2B_0$.

plasma β at the central axis is 5×10^{-3} . The magnetization parameter $\sigma = E_{em}/h$ is about 2 at the

central axis, where E_{em} is the electromagnetic energy density, and $h = \rho c^2 + \gamma p / (\gamma - 1)$ is the specific enthalpy with $\gamma = 4/3$ the adiabatic index.

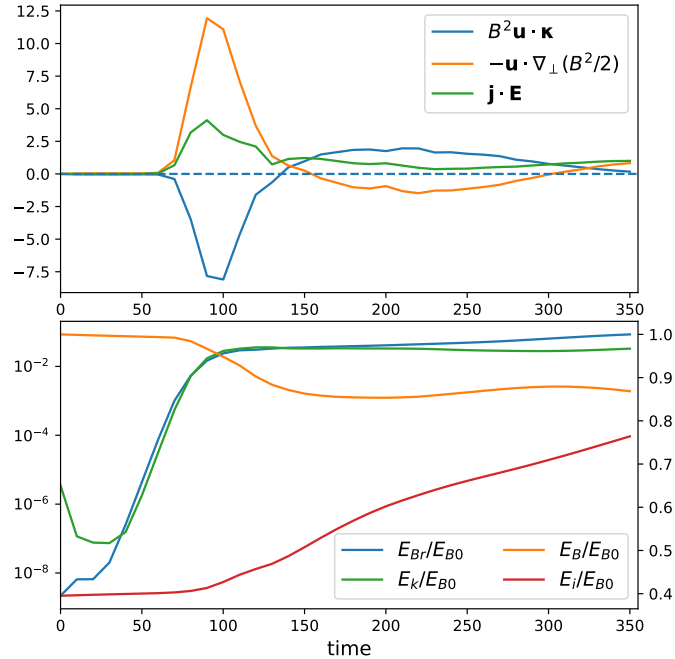


Figure 9. Time history of the energization terms and the energy components similar to Figure 1, but for the kink simulation. The total magnetic energy and the internal energy are plotted in linear scale, and the energy in B_r and total kinetic energy in log scale.

We apply the same analysis as in the reconnection simulation. Similar to Figure 1, we plot the time history of the magnetic energy conversion terms in the top panel of Figure 9. The bottom panel of Figure 9 plots the evolution of energy in the radial component of magnetic field developed from the kink instability. The total magnetic energy, kinetic energy, and internal energy are also plotted in the figure. To avoid the effect of the open boundaries, we restrict the calculation to the region $|x| \leq 10$ and $|y| \leq 10$. At later time $t \gtrsim 200$ (which is 5 light-crossing times in the transverse direction), the total magnetic energy stops decreasing while the total magnetic energy conversion $\mathbf{j} \cdot \mathbf{E}$ is positive, which is likely a boundary effect. Nevertheless, similar to the reconnection case, the system undergoes a rapid instability in the beginning, as illustrated by the exponential increase in the E_{Br} energy before $t \sim 100$. At the later stage of the evolution, the instability saturates and the

system enters a more turbulent state. The top panel of Figure 9 shows that the total energization ($\mathbf{j} \cdot \mathbf{E}$) is nearly zero in the earlier stage and maintains a finite positive value at the later stage. It can also be seen that the CR and PE terms are anti-correlated very well with each other and tend to cancel each other out. This can be understood as both the curvature and gradient vectors of the magnetic field point toward the central axis in a cylindrical kink configuration at zeroth order, so that the two terms in Equation (5) have opposite signs. And it can indeed be verified that $\kappa = \nabla_{\perp}(B^2/2)/B^2$ for the initial kink magnetic field configuration. The finite energization in the later stage is mostly contributed by the CR term, though part of its contribution is canceled out by the PE term. As the kink instability becomes further developed, the $\mathbf{j} \cdot \mathbf{E}$ term shows that the net magnetic energy conversion becomes appreciable after $t \sim 80$ when the PE term becomes the main contributor in the magnetic energy conversion though part of its contribution is canceled out by the CR term. At the later more turbulent stage, the roles of the two terms are reversed and the net magnetic energy conversion rate is reduced.

Similar to Figure 2, we plot the spatial distribution of the conversion terms for the kink simulation, shown in Figure 10. The spatial anti-correlation of the curvature and gradient terms is strong during the initial unstable stage where there is very little net conversion of magnetic energy (the total $\mathbf{j} \cdot \mathbf{E}$ is nearly zero). While more turbulent patterns develop at the later stage, the anticorrelation between the two term is still clear. Although the simulation is not run long enough, we expect that the system will become more turbulent as it evolves further in time.

4. SUMMARY AND CONCLUSIONS

In this paper, the conversion of magnetic energy is discussed in the MHD framework. Both theoretical analysis and numerical simulations are presented, illustrating different mechanisms for the energy transfer. To summarize, our work yields the following conclusions:

1. In the ideal MHD description, the total energy transfer from magnetic energy to plasma energy $\mathbf{j} \cdot \mathbf{E}$ can be separated into two dominant processes. Physically, the first part represents the relaxation of magnetic field line tension when the plasma flow velocity is aligned with the

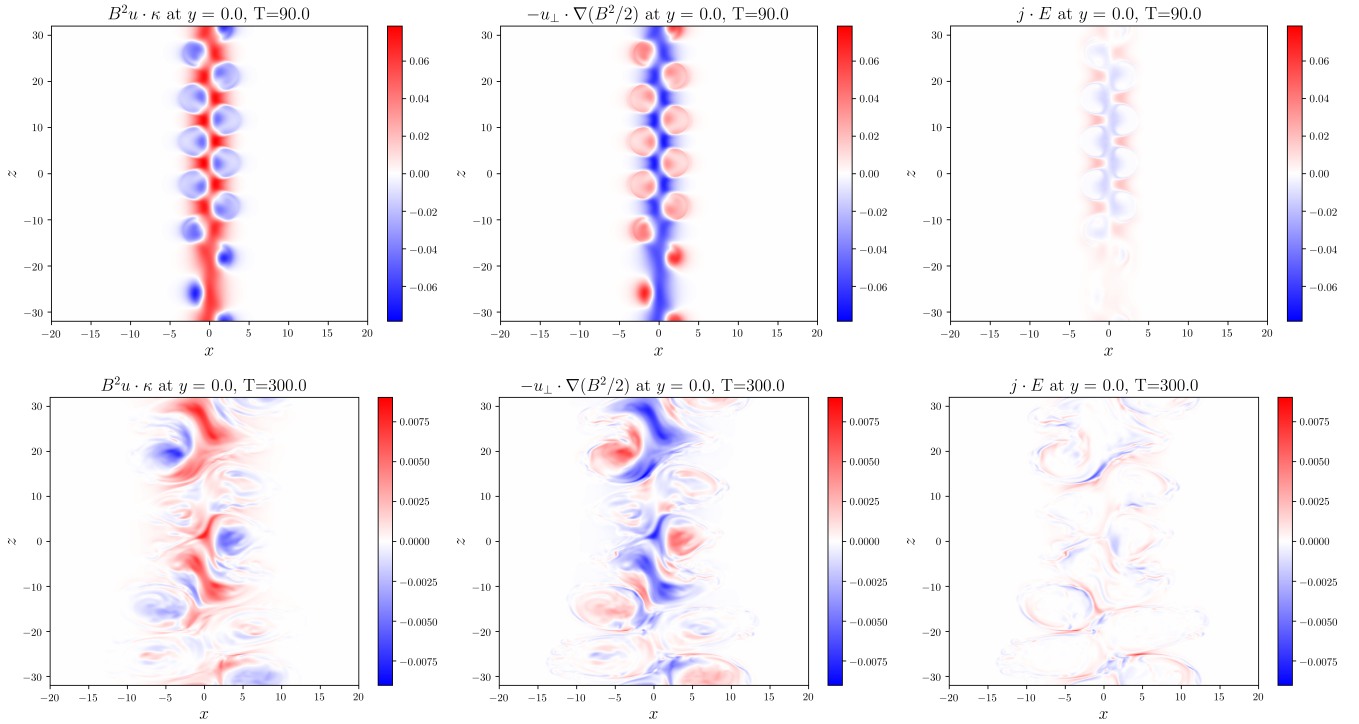


Figure 10. Similar to Figure 2, spatial distribution of the CR (left) and PE (middle) terms and their sum (right) in the x - z plane at early ($t = 90$) and late ($t = 300$) times of the kink simulation. The spatial variation along the jet direction comes from the superposition of modes with different wavelengths.

magnetic field curvature (the CR term); and the second part represents the situation where the perpendicular magnetic pressure gradients are anti-aligned with the plasma flow (the PE term).

2. We present several ideal MHD simulations for two types of systems: magnetic reconnection and kinked jet. We find that, for both 3D reconnection and kinked jet, the CR and PE terms make comparable contributions to the conversion of magnetic energy to plasma energy, with the PE process playing a more important role overall in the magnetic energy conversion.
3. For both 3D reconnection and kinked jet, which have an inherent instability (tearing and kink) to start the magnetic energy conversion process, a quasi-turbulent state is developed as the system evolves further into the nonlinear stage. The relative importance of the CR and PE terms appear to reverse in the turbulent stage compared to the linear stage. For 3D reconnection, the CR term dominates the conversion of magnetic energy to plasma energy in

the beginning while the PE term becomes more important in the later more turbulent stage. For kinked jet, the PE term dominates the magnetic energy conversion at the beginning but the CR term becomes more important later.

4. In the 3D reconnection situation, the relative importance of the CR and PE terms depend on the presence of guide field, most likely due to the impact of the guide field on the strength of perpendicular expansion owing the magnetic pressure gradients. For a finite guide field ($B_g = 0.2$), we find that the CR term is overall the more important term.

These findings are potentially important for understanding particle energization in 3D and over many nonlinear times. The role and importance of the PE term might have been under appreciated previously, particularly given its overall dominance in producing substantially more magnetic energy conversion than the CR term. It will be interesting to explore more in depth its consequences on particle energization and transport processes in 3D magnetically dominated systems.

- 1 We acknowledge the support from a NASA/LWS project 80HQTR20T0027. S.D. and H.L. also
- 2 acknowledge the support by DOE OFES program and LANL/LDRD program. Useful discussions
- 3 with X. Li and F. Guo are gratefully acknowledged. Simulations were carried out using LANL's
- 4 Institutional Computing resources.

REFERENCES

- | | |
|---|--|
| <p>Abdo, A. A., Ackermann, M., Ajello, M., et al. 2011, <i>Science</i>, 331, 739, doi: 10.1126/science.1199705</p> <p>Aharonian, F., Akhperjanian, A. G., Bazer-Bachi, A. R., et al. 2007, <i>ApJL</i>, 664, L71, doi: 10.1086/520635</p> <p>Aluie, H., Li, S., & Li, H. 2012, <i>ApJL</i>, 751, L29, doi: 10.1088/2041-8205/751/2/L29</p> | <p>Bandyopadhyay, R., Yang, Y., Matthaeus, W. H., et al. 2020, <i>ApJL</i>, 893, L25, doi: 10.3847/2041-8213/ab846e</p> <p>Beresnyak, A., & Li, H. 2016, <i>ApJ</i>, 819, 90, doi: 10.3847/0004-637X/819/2/90</p> <p>Bhattacharjee, A., Huang, Y.-M., Yang, H., & Rogers, B. 2009, <i>Physics of Plasmas</i>, 16, 112102, doi: 10.1063/1.3264103</p> |
|---|--|

- Birn, J., Borovsky, J. E., & Hesse, M. 2012, *Physics of Plasmas*, 19, 082109, doi: [10.1063/1.4742314](https://doi.org/10.1063/1.4742314)
- Chew, G. F., Goldberger, M. L., & Low, F. E. 1956, *Proceedings of the Royal Society of London Series A*, 236, 112, doi: [10.1098/rspa.1956.0116](https://doi.org/10.1098/rspa.1956.0116)
- Colgate, S. A., Li, H., & Pariev, V. 2001, *Physics of Plasmas*, 8, 2425, doi: [10.1063/1.1351827](https://doi.org/10.1063/1.1351827)
- Dahlin, J. T., Drake, J. F., & Swisdak, M. 2014, *Physics of Plasmas*, 21, 092304, doi: [10.1063/1.4894484](https://doi.org/10.1063/1.4894484)
- Drake, J. F., Swisdak, M., Che, H., & Shay, M. A. 2006, *Nature*, 443, 553, doi: [10.1038/nature05116](https://doi.org/10.1038/nature05116)
- Du, S., Guo, F., Zank, G. P., Li, X., & Stanier, A. 2018, *ApJ*, 867, 16, doi: [10.3847/1538-4357/aae30e](https://doi.org/10.3847/1538-4357/aae30e)
- Du, S., Zank, G. P., Li, X., & Guo, F. 2020, *PhRvE*, 101, 033208, doi: [10.1103/PhysRevE.101.033208](https://doi.org/10.1103/PhysRevE.101.033208)
- Dungey, J. W. 1961, *PhRvL*, 6, 47, doi: [10.1103/PhysRevLett.6.47](https://doi.org/10.1103/PhysRevLett.6.47)
- Guo, F., Li, H., Daughton, W., & Liu, Y.-H. 2014, *PhRvL*, 113, 155005, doi: [10.1103/PhysRevLett.113.155005](https://doi.org/10.1103/PhysRevLett.113.155005)
- Huang, Y.-M., & Bhattacharjee, A. 2010, *Physics of Plasmas*, 17, 062104, doi: [10.1063/1.3420208](https://doi.org/10.1063/1.3420208)
- . 2016, *ApJ*, 818, 20, doi: [10.3847/0004-637X/818/1/20](https://doi.org/10.3847/0004-637X/818/1/20)
- Hunana, P., Tenerani, A., Zank, G. P., et al. 2019, *Journal of Plasma Physics*, 85, 205850602, doi: [10.1017/S0022377819000801](https://doi.org/10.1017/S0022377819000801)
- Kowal, G., de Gouveia Dal Pino, E. M., & Lazarian, A. 2012, *PhRvL*, 108, 241102, doi: [10.1103/PhysRevLett.108.241102](https://doi.org/10.1103/PhysRevLett.108.241102)
- Kowal, G., Falceta-Gonçalves, D. A., Lazarian, A., & Vishniac, E. T. 2017, *ApJ*, 838, 91, doi: [10.3847/1538-4357/aa6001](https://doi.org/10.3847/1538-4357/aa6001)
- Kronberg, P. P., Dufton, Q. W., Li, H., & Colgate, S. A. 2001, *ApJ*, 560, 178, doi: [10.1086/322767](https://doi.org/10.1086/322767)
- Lazarian, A., Eyink, G. L., Jafari, A., et al. 2020, *Physics of Plasmas*, 27, 012305, doi: [10.1063/1.5110603](https://doi.org/10.1063/1.5110603)
- le Roux, J. A., Zank, G. P., & Khabarova, O. V. 2018, *ApJ*, 864, 158, doi: [10.3847/1538-4357/aad8b3](https://doi.org/10.3847/1538-4357/aad8b3)
- le Roux, J. A., Zank, G. P., Webb, G. M., & Khabarova, O. 2015, *ApJ*, 801, 112, doi: [10.1088/0004-637X/801/2/112](https://doi.org/10.1088/0004-637X/801/2/112)
- Li, H., Lapenta, G., Finn, J. M., Li, S., & Colgate, S. A. 2006, *ApJ*, 643, 92, doi: [10.1086/501499](https://doi.org/10.1086/501499)
- Li, X., Guo, F., Li, H., & Birn, J. 2018, *ApJ*, 855, 80, doi: [10.3847/1538-4357/aaacd5](https://doi.org/10.3847/1538-4357/aaacd5)
- Li, X., Guo, F., Li, H., & Li, G. 2015, *ApJL*, 811, L24, doi: [10.1088/2041-8205/811/2/L24](https://doi.org/10.1088/2041-8205/811/2/L24)
- . 2017, *ApJ*, 843, 21, doi: [10.3847/1538-4357/aa745e](https://doi.org/10.3847/1538-4357/aa745e)
- Li, X., Guo, F., Li, H., Stanier, A., & Kilian, P. 2019, *ApJ*, 884, 118, doi: [10.3847/1538-4357/ab4268](https://doi.org/10.3847/1538-4357/ab4268)

- Loureiro, N. F., Schekochihin, A. A., & Cowley, S. C. 2007, *Physics of Plasmas*, 14, 100703, doi: [10.1063/1.2783986](https://doi.org/10.1063/1.2783986)
- Matthaeus, W. H., Yang, Y., Wan, M., et al. 2020, *ApJ*, 891, 101, doi: [10.3847/1538-4357/ab6d6a](https://doi.org/10.3847/1538-4357/ab6d6a)
- Medina-Torrejón, T. E., de Gouveia Dal Pino, E. M., Kadowaki, L. H. S., et al. 2021, *ApJ*, 908, 193, doi: [10.3847/1538-4357/abd6c2](https://doi.org/10.3847/1538-4357/abd6c2)
- Mizuno, Y., Lyubarsky, Y., Nishikawa, K.-I., & Hardee, P. E. 2009, *ApJ*, 700, 684, doi: [10.1088/0004-637X/700/1/684](https://doi.org/10.1088/0004-637X/700/1/684)
- Nakamura, M., Li, H., & Li, S. 2007, *ApJ*, 656, 721, doi: [10.1086/510361](https://doi.org/10.1086/510361)
- Parker, E. N. 1957, *J. Geophys. Res.*, 62, 509, doi: [10.1029/JZ062i004p00509](https://doi.org/10.1029/JZ062i004p00509)
- . 1963, *ApJS*, 8, 177, doi: [10.1086/190087](https://doi.org/10.1086/190087)
- . 1979, *Cosmical magnetic fields. Their origin and their activity*
- Priest, E., & Forbes, T. 2007, *Magnetic Reconnection*
- Ripperda, B., Bacchini, F., & Philippov, A. A. 2020, *ApJ*, 900, 100, doi: [10.3847/1538-4357/ababab](https://doi.org/10.3847/1538-4357/ababab)
- Sironi, L., & Spitkovsky, A. 2014, *ApJL*, 783, L21, doi: [10.1088/2041-8205/783/1/L21](https://doi.org/10.1088/2041-8205/783/1/L21)
- Stone, J. M., Gardiner, T. A., Teuben, P., Hawley, J. F., & Simon, J. B. 2008, *ApJS*, 178, 137, doi: [10.1086/588755](https://doi.org/10.1086/588755)
- Stone, J. M., Tomida, K., White, C. J., & Felker, K. G. 2020, *ApJS*, 249, 4, doi: [10.3847/1538-4365/ab929b](https://doi.org/10.3847/1538-4365/ab929b)
- Sweet, P. A. 1958, in *Electromagnetic Phenomena in Cosmical Physics*, ed. B. Lehnert, Vol. 6, 123
- Werner, G. R., Uzdensky, D. A., Cerutti, B., Nalewajko, K., & Begelman, M. C. 2016, *ApJL*, 816, L8, doi: [10.3847/2041-8205/816/1/L8](https://doi.org/10.3847/2041-8205/816/1/L8)
- Yang, L., Li, H., Guo, F., et al. 2020, *ApJL*, 901, L22, doi: [10.3847/2041-8213/abb76b](https://doi.org/10.3847/2041-8213/abb76b)
- Yang, Y., Shi, Y., Wan, M., Matthaeus, W. H., & Chen, S. 2016, *PhRvE*, 93, 061102, doi: [10.1103/PhysRevE.93.061102](https://doi.org/10.1103/PhysRevE.93.061102)
- Yang, Y., Wan, M., Matthaeus, W. H., et al. 2019, *Physics of Plasmas*, 26, 072306, doi: [10.1063/1.5099360](https://doi.org/10.1063/1.5099360)
- Zank, G. P., le Roux, J. A., Webb, G. M., Dosch, A., & Khabarova, O. 2014, *ApJ*, 797, 28, doi: [10.1088/0004-637X/797/1/28](https://doi.org/10.1088/0004-637X/797/1/28)
- Zhang, H., Li, H., Guo, F., & Taylor, G. 2017, *ApJ*, 835, 125, doi: [10.3847/1538-4357/835/2/125](https://doi.org/10.3847/1538-4357/835/2/125)

APPENDIX

A. RELATING MAGNETIC ENERGY CONVERSION TO PLASMA ENERGIZATION

The relationship between the CR+PE processes as described in Equation (5) and the plasma energization processes remains, however, relatively unexplored. It is tempting to seek any correspondence between the magnetic energy conversion terms expressed in Equations (5) and (9) with particle energization processes, particularly in the context of the recent kinetic studies (e.g., Li et al. 2017, 2018). We now discuss some possible connections.

A.1. *Single particle drifts and energization*

Beresnyak & Li (2016) have suggested that the particle's curvature drift acceleration could be related to the CR term discussed in Equation (5). The curvature drift velocity of a single particle is

$$\mathbf{v}_c = c \frac{2\mathcal{E}_{\parallel}}{qB} (\mathbf{b} \times \boldsymbol{\kappa}), \quad (\text{A1})$$

where $\mathcal{E}_{\parallel} = mv_{\parallel}^2/2$ is the particle parallel energy. Using the convective electric field, particle acceleration by curvature drift can be obtained by calculating the work done by the electric field on the particle's curvature drift velocity,

$$\left. \frac{d\mathcal{E}}{dt} \right|_c = q\mathbf{E} \cdot \mathbf{v}_c = 2\mathcal{E}_{\parallel} \mathbf{u} \cdot \boldsymbol{\kappa}. \quad (\text{A2})$$

This process was emphasized in Beresnyak & Li (2016). Similarly, using the grad-B drift velocity,

$$\mathbf{v}_g = c \frac{\mathcal{E}_{\perp}}{qB} \frac{\mathbf{B} \times \nabla B}{B^2}, \quad (\text{A3})$$

we find that particle acceleration by grad-B drift as,

$$\left. \frac{d\mathcal{E}}{dt} \right|_g = q\mathbf{E} \cdot \mathbf{v}_g = \frac{\mathcal{E}_{\perp}}{B^2} \mathbf{u} \cdot \nabla_{\perp} \left(\frac{B^2}{2} \right). \quad (\text{A4})$$

This grad-B drift acceleration term was not included in Beresnyak & Li (2016), as they primarily focused on the incompressible MHD limit where the curvature drift term dominates. In a general compressible system, the conclusions of Beresnyak & Li (2016) need to be revisited and expanded.

Equations (A2) and (A4) contain terms $\mathbf{u} \cdot \boldsymbol{\kappa}$ and $\mathbf{u} \cdot \nabla_{\perp} (B^2/2)$, respectively, which are included in the two magnetic energy conversion processes of CR and PE as shown in Equation (5). We have placed these expressions side-by-side for comparison,

$$\begin{aligned} \mathbf{j} \cdot \mathbf{E} &= \frac{B^2}{4\pi} \mathbf{u} \cdot \boldsymbol{\kappa} - \mathbf{u} \cdot \nabla_{\perp} \left(\frac{B^2}{8\pi} \right), \quad \text{magnetic energy conversion rate in MHD (complete)} \\ \frac{d\mathcal{E}}{dt} &\sim 2\mathcal{E}_{\parallel} \mathbf{u} \cdot \boldsymbol{\kappa} + \frac{4\pi\mathcal{E}_{\perp}}{B^2} \mathbf{u} \cdot \nabla_{\perp} \left(\frac{B^2}{8\pi} \right), \quad \text{single particle energy change rate (partial)} \end{aligned} \quad (\text{A5})$$

One has to be very cautious in drawing any conclusions from this seeming similarity. For example, from a single particle perspective, the particle energy gain associated with curvature drift ($d\mathcal{E}/dt|_c > 0$) has the same sign as the CR process with an increase in plasma energy ($\mathbf{j} \cdot \mathbf{E} > 0$). However, the particle energy gain associated with gradient drift ($d\mathcal{E}/dt|_g > 0$) has the *opposite* sign as the PE process with a *decrease* in plasma energy ($\mathbf{j} \cdot \mathbf{E} < 0$). So, we should not directly relate the CR and PE processes in magnetic energy conversion with the curvature drift and grad-B drift processes in particle energization. This is not surprising — an example is that particles gain energy due to gradient drift at a perpendicular shock while the magnetic field energy increases at the shock front. Both particles and magnetic fields gain energy from the bulk flow energy. For the acceleration of energetic particles, Equations (A2) and (A4) show that the energy gained by particles is proportional to the particle (parallel or perpendicular) energy. Therefore, high-energy particles may gain a significant amount of energy via a Fermi-like mechanism upon encountering a region with $\mathbf{u} \cdot \boldsymbol{\kappa} > 0$ or $\mathbf{u} \cdot \nabla_{\perp} B^2 > 0$. This is different from the conversion of magnetic energy in Equation (5), which does not depend on particle energy.

A.2. Particle drift currents and energization

Using the kinetic studies of magnetic reconnection, Li et al. (2018) showed from the Vlasov equation that, in the limit when particles are sufficiently magnetized, the particle energization due to perpendicular electric field can be expressed as the sum of curvature drift, gradient drift, perpendicular magnetization, and bulk acceleration (the inertial term) in the limit of gyrotropic pressure. The curvature and gradient drift terms are found to be dominant over the others (Li et al. 2017, 2018).

Specifically, the energization of particles due to drifts can also be calculated as

$$\mathbf{j}_c \cdot \mathbf{E} = p_{\parallel} c \frac{\mathbf{b} \times \boldsymbol{\kappa}}{B} \cdot \mathbf{E} = p_{\parallel} \mathbf{u} \cdot \boldsymbol{\kappa}; \quad (\text{A6})$$

$$\mathbf{j}_g \cdot \mathbf{E} = (p_{\perp} c \frac{\mathbf{B}}{B^3} \times \nabla B) \cdot \mathbf{E} = \frac{p_{\perp}}{B^2} \mathbf{u} \cdot \nabla_{\perp} \left(\frac{B^2}{2} \right), \quad (\text{A7})$$

where p_{\parallel} and p_{\perp} represent parallel and perpendicular pressure. Fully kinetic PIC simulations have shown that curvature drift acceleration is found to be the dominant particle acceleration mechanism, while grad-B drift typically has the effect of decelerating particles.

By assuming an isotropic pressure, we could use our 3D MHD reconnection simulation described in §3.1 to study the evolution of Equations (A6) and (A7). Figure 11 shows the plasma energy change rates due to curvature and gradient drift currents using Equation (A6) and (A7) assuming an isotropic pressure. The figure shows clearly that the plasma energy gain via curvature drift $\mathbf{j}_c \cdot \mathbf{E}$ remains positive throughout the simulation, while the plasma energy change via the grad-B drift process $\mathbf{j}_g \cdot \mathbf{E}$ is negative for most of the time. The results here are qualitatively similar to those from PIC simulations (Li et al. 2017), indicating that the particle acceleration is perhaps more sensitive to the global field structure rather than the detailed kinetic physics near the reconnection X-line. We have also plotted the total $\mathbf{j} \cdot \mathbf{E}$ (red dashed line) as given in Equation (5). Note that it exhibits difference from the sum of Equations (A6) and (A7) (green curve), indicating that these two processes do not capture the total magnetic energy conversion.

It should be emphasized that the two terms shown in Equations (A6) and (A7) should not be equated to the CR and PE terms in Equation (5). For example, the particle gain via the curvature drift current is proportional to the particle (parallel) pressure whereas the CR magnetic energy conversion term is completely independent of the particle pressure. Intuitively, however, the two descriptions appear to be linked. For a plasma that is approximately in pressure balance, the particle pressure is anti-correlated with the magnetic pressure, so that particles tend to gain a large amount of energy in the high-curvature region where the particle pressure tends also to be high.

As for the grad-B drift term and the PE process, one needs to keep in mind that there is no direct correlation or correspondence between the particle energy change via grad-B drifts and the

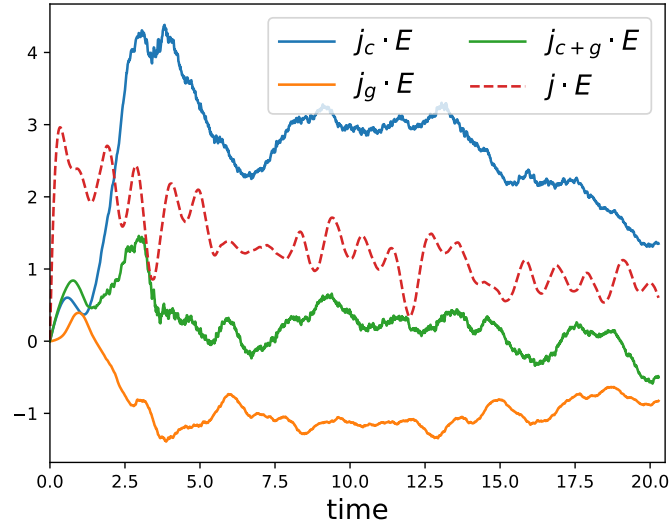


Figure 11. Time history of particle-based energization terms in Equation (A6) and (A7) for the magnetic reconnection simulation. The sum of the two terms is plotted as the green curve ($\mathbf{j}_{c+g} \cdot \mathbf{E}$). The total magnetic energy conversion $\mathbf{j} \cdot \mathbf{E}$ is plotted as the red dashed line for comparison.

magnetic energy change. For example, a decrease in the bulk kinetic flow energy could cause a positive $\mathbf{u} \cdot \nabla_{\perp} (B^2/2)$ so that both the particle energy gain via grad-B and the magnetic energy increase can occur.